CHEMICAL ENGINEERING TRANSACTIONS
VOL. 99, 2023
A publication of AIDIC
The Italian Association of Chemical Engineering
Online at www.cetjournal.it
Guest Editors: Sauro Pierucci, Flavio Manenti

ISBN 978-88-95608-98-3; **ISSN** 2283-9216
DOI: 10.3303/CET2399020

Gasification Of Wood Powder in a Small-Scale Entrained Flow Gasifier

Roger A. Khalil*, Morten Seljeskog, Jørn Bakken, Øyvind Skreiberg

Thermal Energy Department, SINTEF Energy Research, Trondheim, Norway
Roger.A.Khalil@sintef.no

Gasification of wood powder milled from commercially available wood pellets have been performed in a small-scale entrained flow gasifier. The main aim of this study is to investigate operational and feedstock requirements (mainly particle size distribution, (PSD)) for this small-sized gasifier to perform with good carbon conversion ratio. The effects of several parameters were investigated, resulting in variable performance. The investigated parameters were equivalence ratio (lambda, λ), oxidant type (air or oxygen), thermal load, pressure, burner head configuration and PSD. The syngas quality, defined as cold gas efficiency (CGE) and/or carbon conversion efficiency (CC) was reported as function of the above parameters. The gasifier achieved a satisfactory conversion when using oxygen as oxidant and at elevated pressure (8.2 bar(a)).

1. Introduction

In Norway, about 3.7 million m^3 of forest residues are left in the forest after harvest yearly, without including natural felling (Bergseng et al., 2013). Also, waste wood from households and industrial activities are the third largest waste stream in Norway with an annual generation of 800,000 tons, about 2.6 million m^3/y. One important incentive for meeting Norway's ambition regarding increased renewable energy should be to find the proper means for the available biomass to be used. One potent chain would be to produce liquid biofuels for the aviation sector which could be achieved through entrained flow gasification of sustainable feedstocks such as biomass. Entrained Flow Reactors (EFRs) using coal as fuel are regarded as a proven technology with many large-scale units in operation (Breault, 2010), and industrial plants developed after 1950 are mostly based on this principle (Higman and Burgt, 2008). However, for biomass and alternative low-grade fuels (high ash content) the technology is still in the development stage. EFRs are generally operated in slagging mode, meaning that the operating temperature is above the ash melting point of the feedstock. At this temperature, tars are destructed, and the fuel is almost fully converted. Among existing gasification technologies, the EFR technology produces the highest syngas quality, i.e. tar free syngas mainly composed of CO and H_2 (Higman and Burgt, 2008; Weiland et al., 2015, 2013). Many advantages can be attributed to EFRs, among the most important being high operating pressure, high gasification temperature and short residence time, a combination that allows for the design of compact reactors (Coda et al., 2007; Tremel et al., 2012). Due to short residence times, usually a few milli seconds, the EFR requires a fuel which has been mechanically processed (grinding, milling etc.) down to powdery sized particles to achieve full conversion within the hot temperature zone. Weiland et al. have investigated the gasification of wood powder in an oxygen blown entrained flow gasifier (Weiland et al., 2015, 2013). Several parameters were investigated to optimize the process, among these are equivalence ratio (lambda), oxidant type (air or oxygen), thermal load, pressure, and PSD of the wood powder. Beech sawdust was gasified in two drop tube setups where also several parameters affecting the conversion process were investigated (Billaud et al., 2016; Qin et al., 2012). In another work, the syngas quality was studied by varying reactor temperature, steam/carbon ratio, and the ratio of the actual oxidant to the stoichiometric one (lambda) for both beech sawdust and straw dust (Qin et al., 2012). It was found that higher amounts of tars in the syngas were present at low gasification temperatures (1000 °C) while at high temperatures (1350 °C) significant amounts of soot was produced and almost no tars.

Paper Received: 17 January 2023; Revised: 13 March 2023; Accepted: 6 May 2023
Please cite this article as: Khalil R.A., Seljeskog M., Bakken J., Skreiberg O., 2023, Gasification of Wood Powder in a Small-scale Entrained Flow Gasifier, Chemical Engineering Transactions, 99, 115-120 DOI:10.3303/CET2399020

In the present study, the gasification efficiency of pulverized commercial pellet fuel in a laboratory scale EFR (12-15 kW) is investigated. Several operating parameters were investigated including lambda, residence time (varied through thermal input, pressure, and oxidant composition), and PSD.

2. Methods and materials

Pellets, made from pine and spruce stemwood sawdust, was milled, and used as feedstock in the current work. To mill the pellets, a hammermill (MAFA EU-4B) with a 0.75 mm sieve was used, producing a powder with mass median diameter, d_{50}, of about 300 µm. The major elements and the ash composition of the feedstock are presented in Table 1 along with the fuel proximate analysis and the heating value.

Table 1: Proximate and ultimate analysis and heating value of the studied feedstock.

Element	Composition	Unit	Element	Composition	Unit
Moisture	5.4	wt-%		Ash composition	
Ash	0.5	wt-% d.s.[1]	Ca	1020	mg/kg d.s.
Volatiles	84.9	wt-% d.s.	K	454	mg/kg d.s.
Fixed Carbon	14.6	wt-% d.s.	Mg	161	mg/kg d.s.
Lower Heating Value	19.18	MJ/kg d.s.	Na	102	mg/kg d.s.
C	50.8	wt-% d.s.	Mn	95.2	mg/kg d.s.
H	6.1	wt-% d.s.	Si	81.7	mg/kg d.s.
N	<0.1	wt-% d.s.	P	40.7	mg/kg d.s.
O	42.5	wt-% d.s.	Al	25.7	mg/kg d.s.
Cl	<0.01	wt-% d.s.	Fe	13.6	mg/kg d.s.
S	0.034	wt-% d.s.	Zn	9.36	mg/kg d.s.

[1]wt-% d.s. = weight percent of dry substance

The PSD of the original feedstock was further changed through additional grinding. This resulted in the PSD (P1 – P3), with these characteristics: P1 is the original feedstock, P2 is a finer fraction of P1 after separation using a sieve with a mesh size 0.63 mm and P3 was prepared by grinding P1 in an attritor type mill. The mill was operated in a batch mode at 460 rpm for 10 minutes. The mill container was filled with 3 liters of P1 particles in addition to 20 kg of 6 mm steel marbles. The PSD of all three biomass powders can be seen in Figure 1. This figure also shows the PSD of P2a which was the coarse fraction after P1 was sieved. P2a was not used in the gasification experiments, however its presence in the figure is for comparative reasons. Due to the nature of the fibrous biomass particles, also characterized by their elongated form, it was difficult to separate the different sizes through sieving. The PSD of P1 and P2 were similar however P2 had a smaller fraction of larger sized particles as stated in Figure 1. P2a had a much lower fraction of smaller sized particles in the range of 1 – 40 µm. The decrease in the number of particles in the range 5 – 200 µm for P2a does not result in a similar increase in P2 and relative to P1. The measurement of PSD was performed in a Mastersizer 3000, an optical instrument which measures particles suspended in gas or liquid. It is interesting to notice that P1 and P2 have a similar PSD while P3 is different. P3 has a PSD profile that spans more evenly across the entire size range.

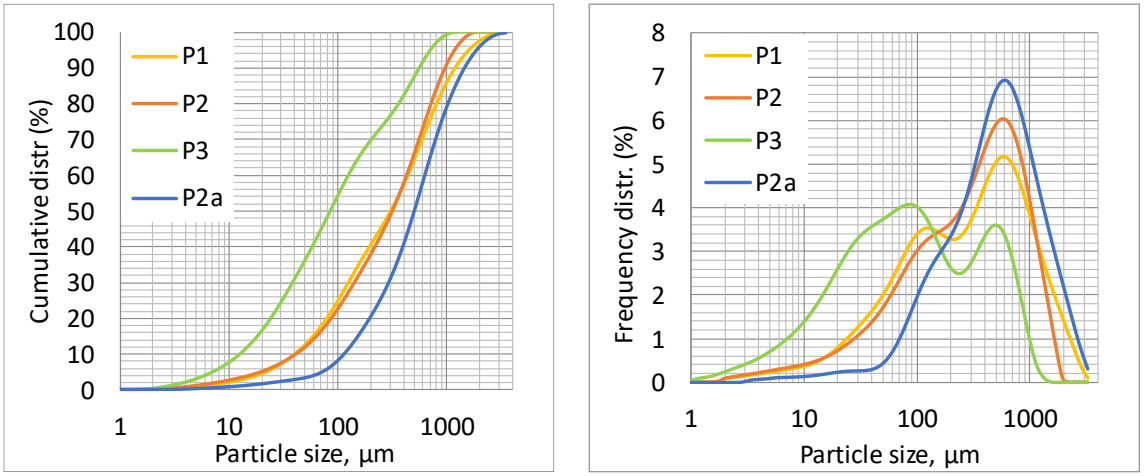

Figure 1: PSD for the powders used in this study, cumulative (left) and particle number (right).

2.1 Experimental setup

The EFR was built with most of the sub-systems found in a full-scale gasification plant. The EFR operated with a fuel feed variation corresponding to 10 – 20 kW, allowing for the detailed study in a smaller setting. A “loss in weight-based” screw feeding system continuously fed biomass particles from a closed hopper to the center of the burner head at the top. The fuel storage hopper was 50 liters in size, allowing for around 8 hours of continuous operation. The reactor itself, and the subsequent coolers were all designed for a maximum of 10 $bar_{(a)}$ operating pressure. The cooling system comprises two sub-systems, a radiative cooler followed by a convective cooler with a combined cooling capacity of about 60 kW. After syngas cooling, propane was added, and the syngas was combusted in a gas burner after which the flue gas was ejected over the roof. A schematic drawing of the EFR along with all its sub-systems is shown in *Figure 2a*. The inner diameter of the reactor is 200 mm, and has a height of 800 mm, *Figure 2c*. The slag/ash/unconverted materials are collected in a container at the bottom outlet after the main cooler. All thermocouples are situated inside the refractory and do not penetrate the inner core wall. TC16 is used to regulate the temperature according to a predefined setpoint by controlling the electrical power to the heating elements and TC14 is used as control for overheating. Six electrically heated elements, type Kanthal Super 1700 918, Lu '440', are equally distributed inside the reactor refractory to preheat the reactor core gas volume to the desired temperature before the start of an experiment and maintain this temperature during the gasification experiment. The reactor was heated at maximum 100 °C/h overnight to the desired gasification temperature. The gasification agent was supplied through individual gas cylinders for the pure gas compounds, i.e., oxygen and nitrogen. The ratio O_2/N_2, including the nitrogen used for purging the fuel feeding system, was equal to that of air except for the oxygen blown experiments. The thermal input varied between 10 – 21 kW, and the oxidant burner velocity varied between 2.5 – 48.3 m/s depending on thermal input, oxidant type, reactor pressure and the burner ring type. The mean residence time in the reactor, calculated as dry gaseous volume flow divided by reactor volume, varied between 1.5 – 22 s. The burner heads had an outlet diameter of 56 mm and was enclosed in a water-cooled jacket, with an inner diameter of 17.3 mm. The fuel is introduced into the reactor through a center tube using between 30-60 Nl/min of nitrogen. The experimental study was performed at different conditions all summarized in Table 2. Exp #1-10 were performed with variable PSD (P1-P3), the “original” burner ring and at atmospheric pressure. Exp #11-17 were performed with a modified burner ring, meant to increase the burner velocity, and introduce swirled mixing (see *Figure 2b*) with a slight increased pressure. Exp #18-21 are performed with a constant thermal input but with decreasing pressure of 7.1-1.2 bars, “original” burner ring and air as gasification agent. Exp #22-25 are performed at constant pressure (8.2 bars) and with pure oxygen passing through the burner head, however nitrogen was still used as a carrier gas to feed the particles in the reactor. These experiments were performed with a special burner ring designed for oxygen gasification (See Figure 2b). Finally, a gas chromatograph of type Varian CP-4900 was used for measuring the syngas composition.

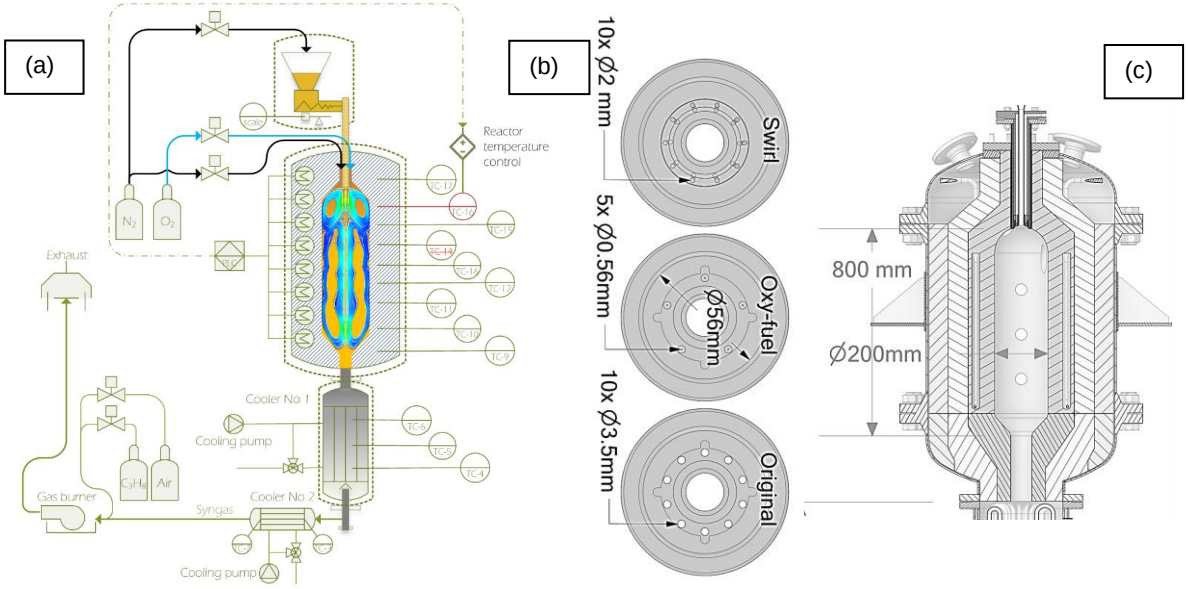

Figure 2: a) A P&ID schematic presentation of the EFR b) burner rings applied c) reactor core

Table 2: Experimental conditions.

Exp. #	Series	Fuel input (kW)	Lambda, λ	Burner velocity (m/s)		Reactor T (°C)	Reactor residence time (s)	Pressure ($bar_{(a)}$)
				Oxidant	Fuel			
1	P1	12.7	0.38	8.1	2.3	1155	3.5	1
2	P1	19.0	0.38	15.6	2.3	1163	2.3	1
3	P1	10.7	0.54	12.2	2.3	1152	3.0	1
4	P1	15.5	0.57	21.8	2.3	1162	2.1	1
5	P2	11.0	0.53	12.2	2.3	1157	3.0	1
6	P2	16.1	0.55	21.9	2.3	1163	2.0	1
7	P2	21.3	0.56	31.2	2.3	1165	1.5	1
8	P3	16.2	0.54	21.7	2.3	1185	3.8	1
9	P3	10.1	0.57	12.2	2.3	1185	5.8	1
10	P3	10.7	0.54	12.2	2.3	1186	6.4	1
11	P1(NR)	15.7	0.57	47.7	2.0	1139	2.2	1
12	P1(NR)	12.8	0.70	45.9	1.9	1144	2.4	1.2
13	P1(NR)	17.9	0.50	44.1	1.9	1146	2.3	1.2
14	P1(NR)	12.6	0.55	30.0	1.9	1148	3.0	1.2
15	P1(NR)	10	0.66	27.0	1.7	1152	3.5	1.3
16	P1(NR)	15.5	0.69	48.3	1.6	1155	2.3	1.4
17	P1(NR)	15.8	0.48	32.4	1.8	1154	2.8	1.3
18	P1(P)	15.8	0.56	2.46	0.32	1138	13.7	7.1
19	P1(P)	15.7	0.56	3.41	0.44	1142	9.7	5.1
20	P1(P)	15.8	0.56	5.56	0.72	1147	5.9	3.1
21	P1(P)	15.6	0.57	15.19	1.96	1151	2.2	1.2
22	P1(O)	12.0	0.58	34.9	0.5	1158	22.3	8.2
23	P1(O)	12.1	0.65	39.9	0.5	1158	22.0	8.2
24	P1(O)	12.2	0.45	28.1	0.6	1148	21.7	8.2
25	P1(O)	14.1	0.56	39.9	0.5	1152	20.6	8.2

2.2 Results and discussions

The lines in all figures represent the linear trendline of all data and are not meant as to show a particular trend. They are however useful to evaluate if a certain cluster is performing better compared to the average value. Data points above that line would mean that the data measured are above the average, while those under the line represent data below average. The CGE for all performed experiments are presented in Figure 3, as a function of CC (left) and λ (right). From the left-hand side figure, we can see that the experiments (P1) have CC rate close to 60%, yielding CGE lower than 20%. P2 having a smaller size distribution has better CC rates while P3 with the much smaller particles compared to P1 and P2 has a CC rate above 90%. However, all these experiments have a CGE below average. This behavior suggests poor mixing conditions between the reactants leading to zones rich in oxygen and probably combustion conditions, thus the low CGE. The experiments marked P1(P) were conducted next with variable pressure. The elevated pressure resulted in a longer residence and more favorable gasification conditions. However, the burner velocity drops down dramatically with increased pressure, resulting in poorer mixing.

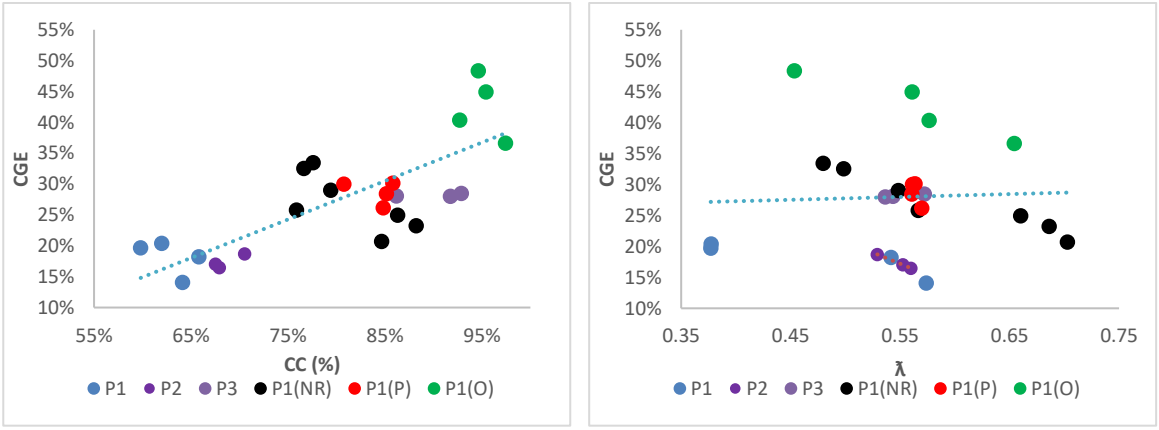

Figure 3: CGE for all experiments as a function of CC (left) and λ (right).

Despite this, Figure 3 shows similar CGE for the P3 but with lower CC rate. Experiments marked P1(NR) were run next using a new burner ring that would give a swirl and have higher velocity compared to the original setup. Two clusters of data can be noticed, the left cluster having CC values close to 80% and CGE above the trendline and the right cluster with higher CC values and lower CGE. The later cluster is run at much higher λ values as *Figure 4* indicates. It is worth mentioning that the CGE decreases with increased λ value for all performed experiments. Finally, P1(O) were performed at elevated pressure, with a specially designed burner head yielding ideal velocities with pure oxygen. For this setup the gasifier performed best compared to all previous experiments. *Figure 4* (left) shows the CC as a function of λ. As a general observation, the CC rate increases with increased λ, which is logical as the more oxidant is introduced to the system, the more carbon is converted. For the last series (P1(O)), the CC is maintained at high levels even at lower λ values. The H_2/CO ratio is an important parameter for evaluating the syngas quality, especially in the case of liquid biofuels production. *Figure 4* (right) shows this ratio for all the experiments performed and as a function of λ. This ratio lies between 0.5-0.6 for most series except for P1 and P2. The highest ratio is obtained with the P1(P) series.

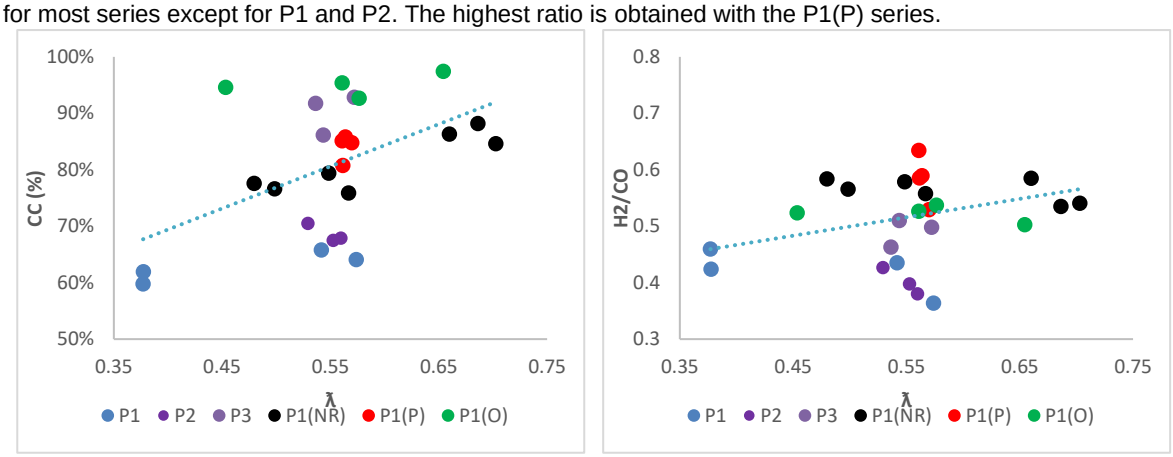

Figure 4: CC (left) and H_2/CO (right) for all experiments as a function of λ.

Figure 5 shows the hydrogen and carbon monoxide concentrations in mol per kg fuel as a function of λ. These concentrations decrease with increasing λ for the different series. Best performance is obtained during the P1(O) series, yielding concentrations well above the rest. For the P1(NR) series, both H_2 and CO concentration are low despite a somehow higher CGE value, depicted in Figure 3. The higher CGE value for this series is due to a slightly higher methane concentration, for the lower λ range which can be seen in Figure 6. The poorest H_2 and CO concentration belong to the P1 and P2 series while P3 and P1(P) are yielding average concentrations.

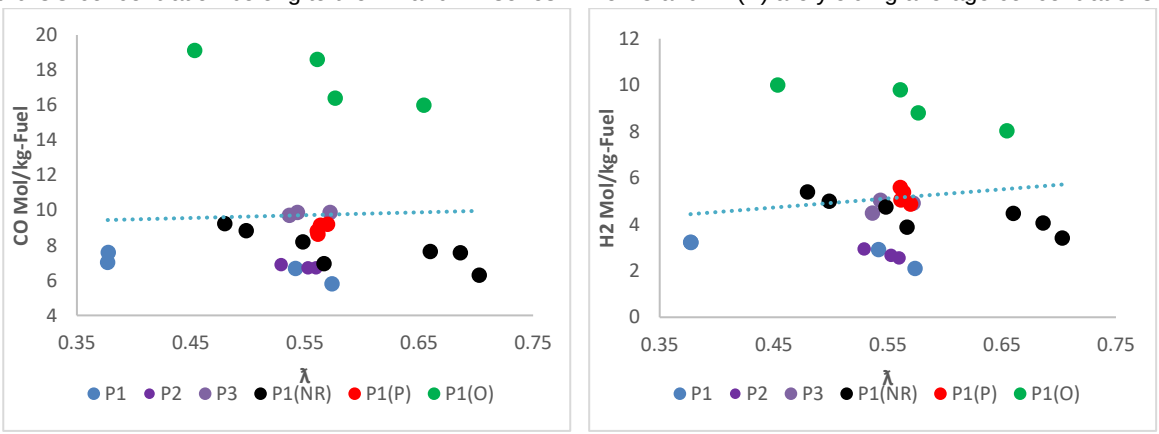

Figure 5: Hydrogen (right) and carbon monoxide (left) concentrations in Mol/kg-Fuel.

Figure 6 shows the methane (left-hand side) and the carbon dioxide (right hand side) concentrations. For the methane, the concentrations are decreasing with increased λ, while for CO_2 the opposite is true. P1, P2 and partially P3 are producing lower methane concentrations compared to the rest of the series. An interesting observation is the methane concentration for the P1(P) series performed with variable reactor pressure. As the upper right corner of Figure 6 (left) indicates, there seem to be a linear dependence between the reactor pressure and the methane concentration at the investigated range. The data points for CO_2 concentration are more concentrated around the trend line except for P3.

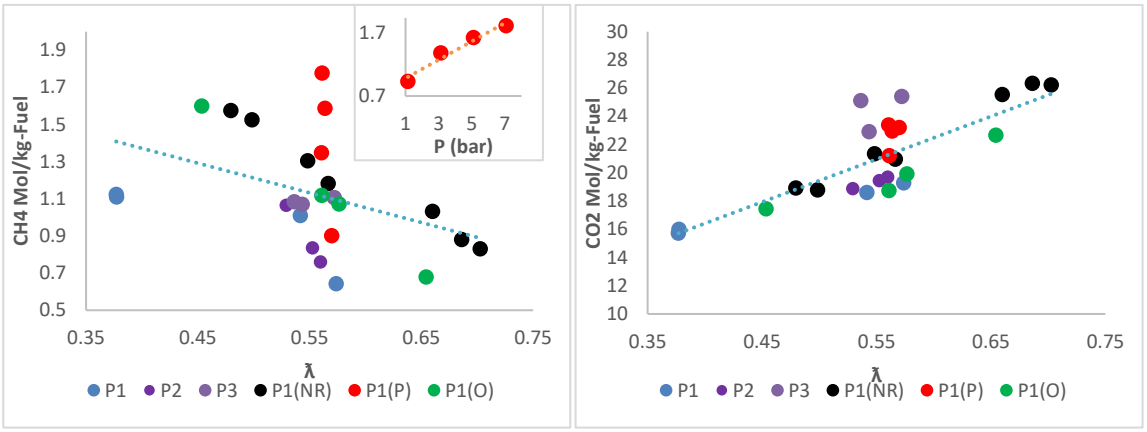

Figure 6: Methane (left) and carbon dioxide (right), concentrations in Mol/kg-Fuel.

3. Conclusions

Gasification of wood powder has been studied in an EFR with a thermal throughput of 10-20 kW. The results were evaluated by measuring key parameters such as CGE and syngas composition. Among the investigated parameters are the PSD of the input fuel, reactor pressure, burner design and reactant composition (air vs oxygen). Two main findings regarding the effect of the PSD are: a) the removal of the largest particles in the original PSD by sieving gave no improvement on the conversion rate, b) but further milling the wood powder had a noticeably better CGE compared to the original powder. Improvement in the burner head design while still using the original wood powder at ambient pressure and air as the gasification agent gave similar results to the extra milled feedstock. Also increasing the pressure, and thereby residence time, while still using air as oxidant gave significant improvement on the gasification efficiency. However, these experiments were performed with an atmospheric burner head, resulting in relatively low velocities through the burner at pressurized conditions. So, the efficiency could be further improved by using a better burner design, suited for pressurized air gasification. This study has enabled the determination of feedstock and operational boundary conditions for producing high quality syngas with good carbon conversion ratio in a small-sized EFR.

Acknowledgments

This work was supported by the Research Council of Norway and several industrial partners through the project "Gasification and FT-Synthesis of Lignocellulosic Feedstocks" (GAFT, 244069), “Next generation Biogas production through the Synergetic Integration of Gasification” (BioSynGas, 319723) and the Centre for Environment-friendly Energy Research (FME) Bio4Fuels.

References

Bergseng, E., Eid, T., Løken, Ø., Astrup, R., 2013. Harvest residue potential in Norway – A bio-economic model appraisal. Scandinavian Journal of Forest Research 28, 470–480.

Billaud, J., Valin, S., Peyrot, M., Salvador, S., 2016. Influence of H_2O, CO_2 and O_2 addition on biomass gasification in entrained flow reactor conditions: Experiments and modelling. Fuel 166, 166–178.

Breault, R.W., 2010. Gasification Processes Old and New: A Basic Review of the Major Technologies. Energies 3, 216–240.

Coda, B., Cieplik, M.K., de Wild, P.J., Kiel, J.H.A., 2007. Slagging Behavior of Wood Ash under Entrained-Flow Gasification Conditions. Energy Fuels 21, 3644–3652.

Higman, C., Burgt, M. van der, 2008. Gasification, 2nd ed. Gulf Professional Pub./Elsevier Science, Amsterdam.

Qin, K., Lin, W., Jensen, P.A., Jensen, A.D., 2012. High-temperature entrained flow gasification of biomass. Fuel 93, 589–600.

Tremel, A., Stemann, J., Herrmann, M., Erlach, B., Spliethoff, H., 2012. Entrained flow gasification of biocoal from hydrothermal carbonization. Fuel 102, 396–403.

Wågønes, T., Sørensen, G., Syversen, F., Materialgjenvinning av returtrevirke (No. 06/2018), Avfall Norge.

Weiland, F., Hedman, H., Marklund, M., Wiinikka, H., Öhrman, O., Gebart, R., 2013. Pressurized Oxygen Blown Entrained-Flow Gasification of Wood Powder. Energy Fuels 27, 932–941.

Weiland, F., Wiinikka, H., Hedman, H., Wennebro, J., Pettersson, E., Gebart, R., 2015. Influence of process parameters on the performance of an oxygen blown entrained flow biomass gasifier. Fuel 153, 510–519.